SUPPORTING INFORMATION

Correlation between fringe spacing in TEM and 2θ value of diffraction peaks in XRD. The relationship between lattice spacings seen in TEM and characteristic reflections in XRD patterns was determined by using Bragg's law:

$$n\lambda = 2d \sin\theta$$

where n is a natural number, λ is the x-ray radiation wavelength (λ = 1.54178 Å), d is the lattice spacing seen in TEM images and θ is the diffraction angle in degrees, whose value multiplied by 2 appears in the XRD patterns.

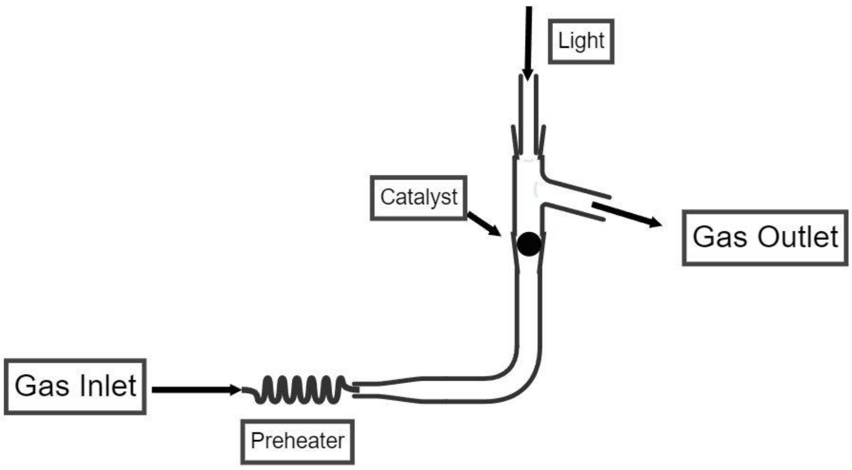

Scheme S1. Reactor setup for photo-assisted CO_2 hydrogenation.

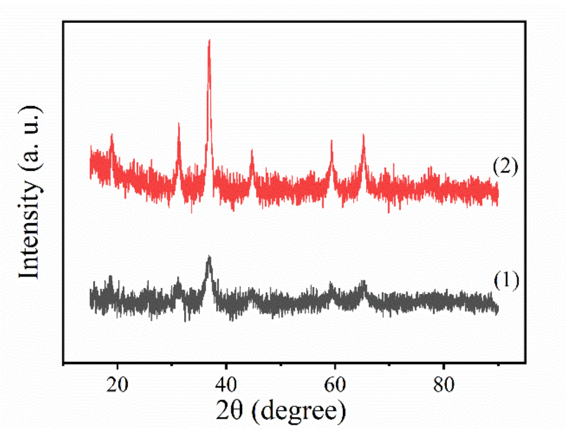

Figure S1. XRD pattern of CoTiAl-FLc (1) and CoTi-MO (2).

Table S1. Cationic ratios of reference samples CoTiAl-FLc and CoTi-MO obtained by EDX.

	MATERIAL	
	CoTiAl-FLc	CoTi-MO
Co (%)	65.5	62.2
Ti (%)	16.5	37.8
Al (%)	18.0	/
Metal Ratio	2:0.5:0.5	1.6:1

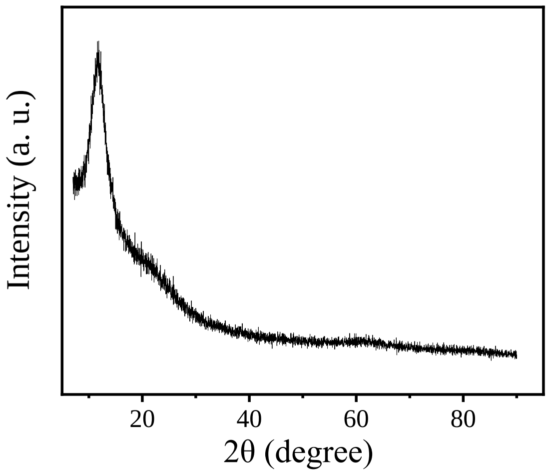

Figure S2. XRD pattern of CoTiAl-LDH intermediate originated at short synthesis times (2h).

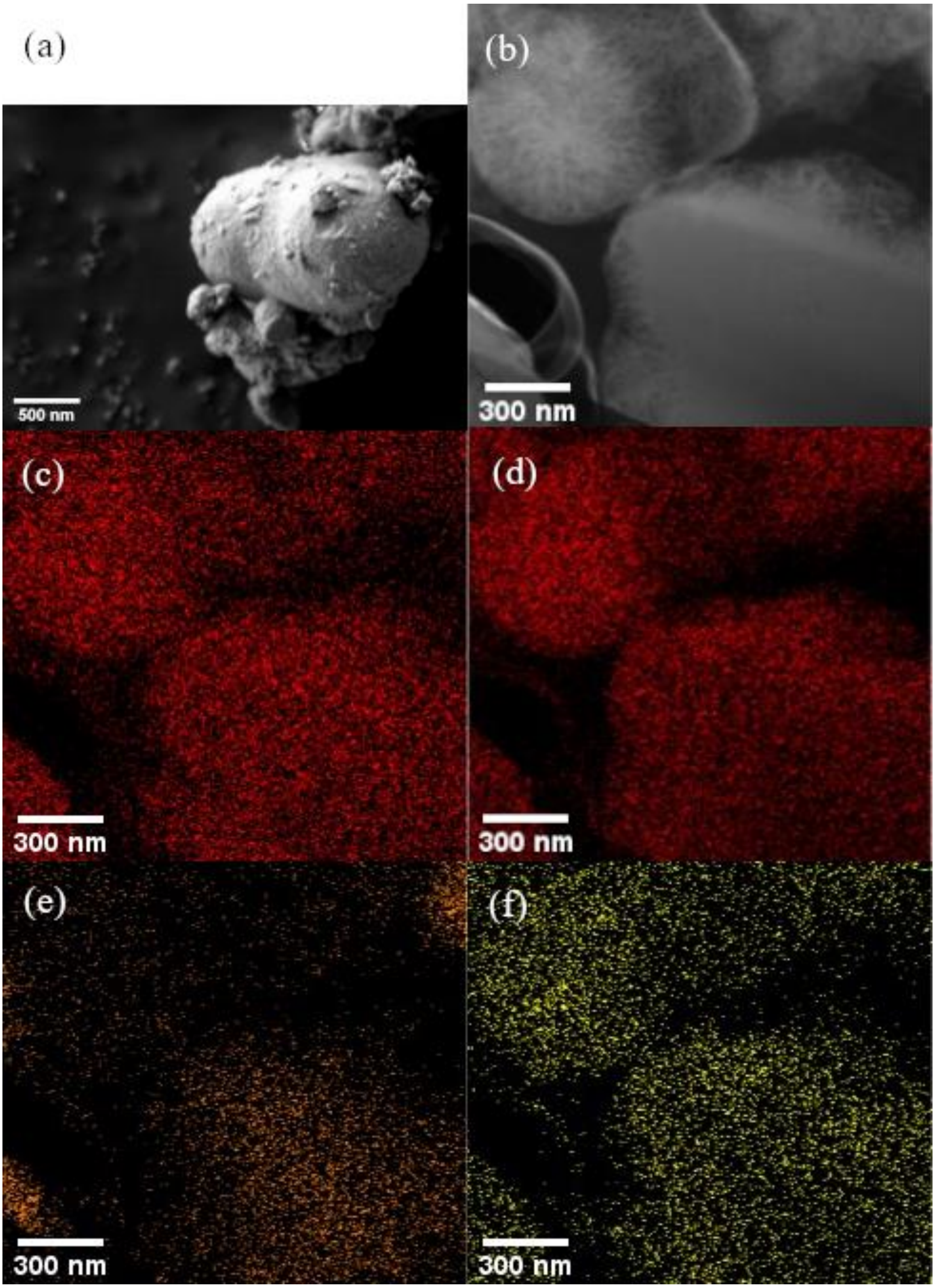

Figure S3. SEM image of CoTiAl-LDH intermediate (a) after 2h of synthesis. STEM image (b) and elemental mapping for O (c), Co (d), Ti (e) and Al (f) of CoTiAl-MO lamellar cross-sections.

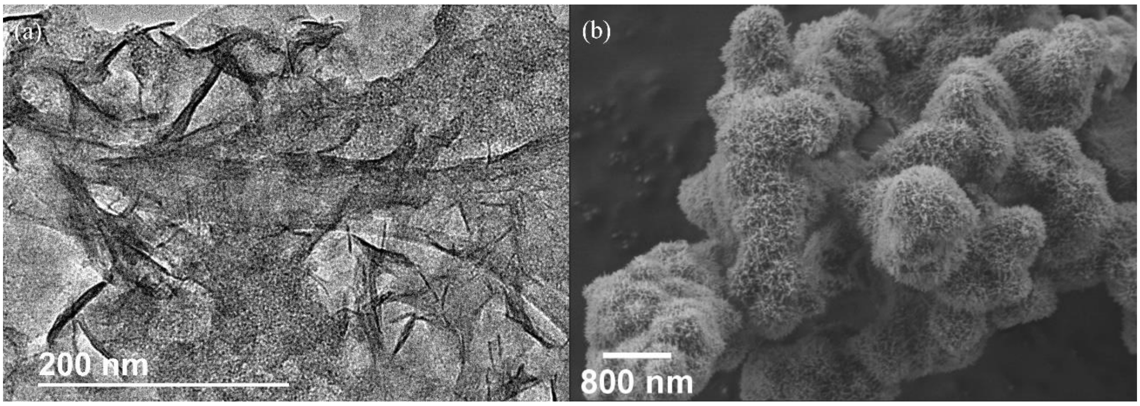

Figure S4. TEM image of CoTiAl-FLc (a). SEM image of CoTi-MO (b).

Table S2. Cationic ratios present in CoTiAl-LDH at different synthesis times obtained by EDX analysis.

Time (h)	% Co	% Ti	% Al
2	4.4	82.5	13.1
24	62.0	19.4	18.6

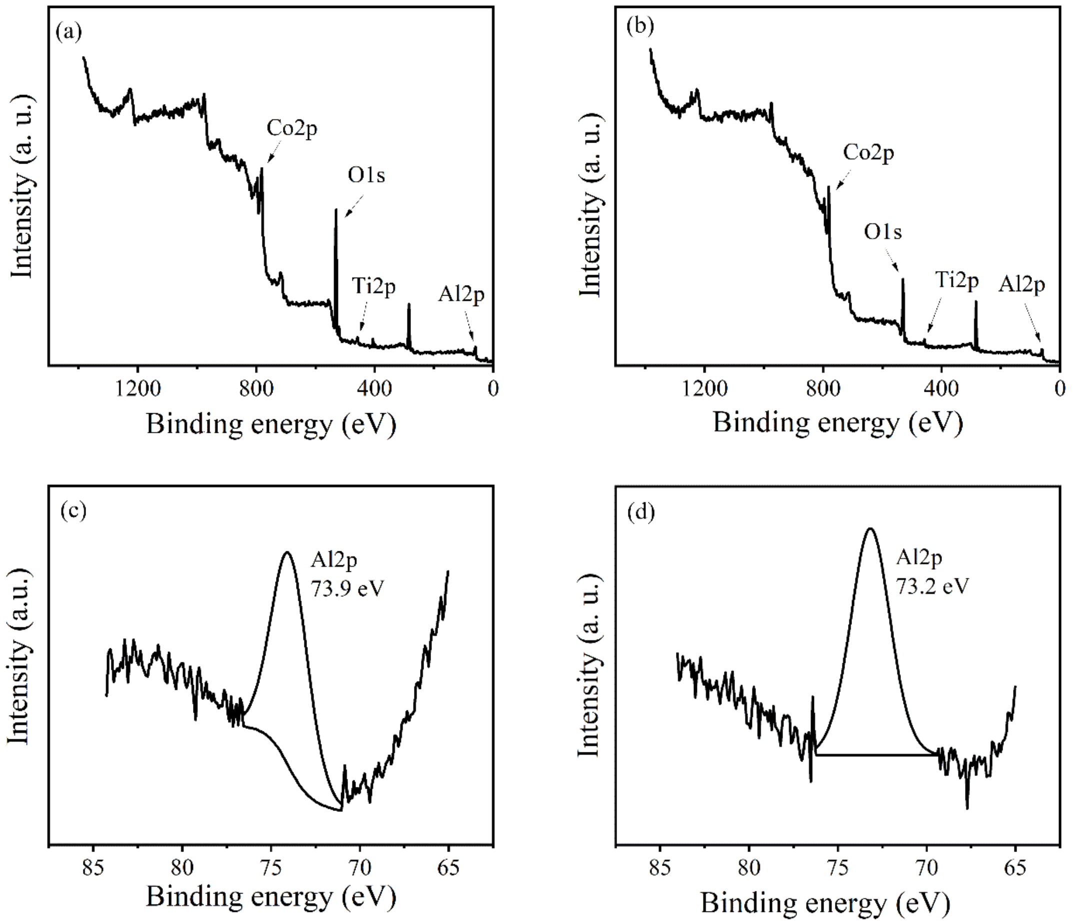

Figure S5. Survey XPS spectra of CoTiAl-LDH (a) and CoTiAl-MO (b). Al2p XPS spectra of CoTiAl-LDH (c) and CoTiAl-MO (d).

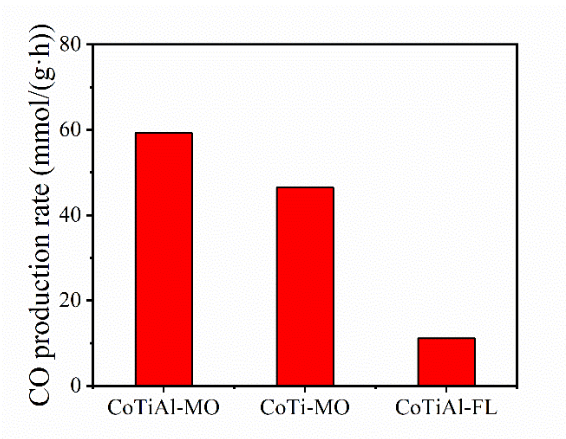

Figure S6. CO production rate over CoTiAl-MO and the reference materials prepared in this work. Reaction conditions: CO_2 + H_2 flow (1:1 ratio, 13 ml/min), T: 200 ºC, UV-Vis irradiation (108 mW/cm^2), 50 mg photocatalyst.

Table S3. State of the art for photo-assisted CO_2 hydrogenation both in batch and flow conditions.

Catalyst	**Reaction conditions**	**Light Source**	**Production ($mmol \cdot g^{-1} \cdot h^{-1}$)**	**Selectivity (%)**	**Ref.**
In_2O_{3-x} nanosheets	Batch No external heating 0.1 MPa	300 W Xe lamp	103.21 (CO)	~100	[1]
In_2O_3/$In2O_{3-x}$	Batch No external heating 0.2 MPa	300 W Xe lamp (2 W/cm^2)	23.87 (CO)	100	[2]
$In_2O_{3-x}(OH)_y$/ $TiN@TiO_2$ NT	Batch No external heating 0.12 MPa	300 W Xe lamp (1 W/cm^2)	81.1 (CO)	99.7	[3]
FeO-CeO_2	Batch No external heating 0.18 MPa	300 W Xe lamp (2.2 W/cm^2)	19.61 (CO)	99.87	[4]
Ru@FL-LDHs	Flow No external heating 0.1 MPa	300 W Xe lamp (1 W/cm^2)	277 (CH_4)	99.3	[5]
Ru/TiO_2	Flow 300 °C 0.1 MPa	500 W Solar Simulator (0.1 W/cm^2)	69.49 (CH_4)	100	[6]
Rh/Al nanoantenna	Batch 200 °C 1.5 MPa	Solar simulator (11.3 W/cm^2)	550 (CH_4)	100	[7]
Rh/TiO_2	Flow 250 °C 0.1 MPa	300 W Xe lamp (2.7 W/cm^2)	20.6 (CO)	100	[8]
Co_{15}HAP	Flow 400 °C 0.1 MPa	300 W Xe lamp (0.1 W/cm^2)	62 (CO)	83	[9]
CoTiAl-MO	**Flow 200 °C 0.1 MPa**	**300 W Xe lamp (0.1 W/cm^2)**	**59.28 (CO), 23.52 (CH_4)**	**71.6 (CO), 28.4 (CH_4)**	**This work**

Table S4. Apparent activation energy values for CO_2 hydrogenation over CoTiAl-MO catalyst in the dark and under irradiation. Reaction order for CO_2 and H_2 under the same conditions are also listed. Reaction conditions: CO_2 + H_2 flow (1:1 ratio, 13 ml/min), 200 °C, UV-vis irradiation (108 mW/cm^2), 50 mg photocatalyst.

		CO	CH_4	CO_2	H_2
Activation Energy (kJ/mol)	Dark	66.065	62.218	/	/
	Light	14.395	9.435	/	/
Reaction Order	Dark	/	/	1.27	0.83
	Light	/	/	1.19	0.68

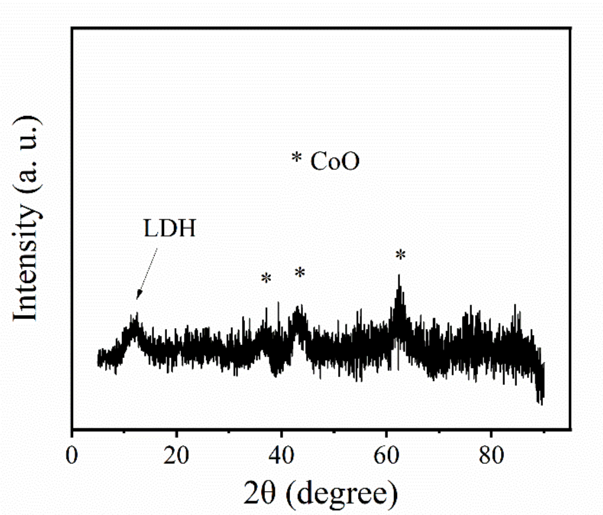

Figure S7. XRD pattern of CoTiAl-MO after 108 h photocatalytic test.

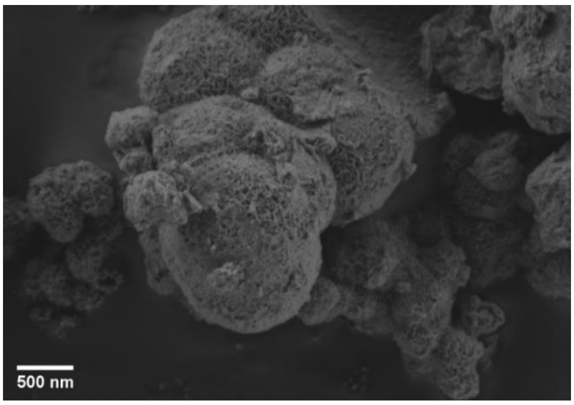

Figure S8. SEM image of CoTiAl-MO after 108 h photocatalytic test.

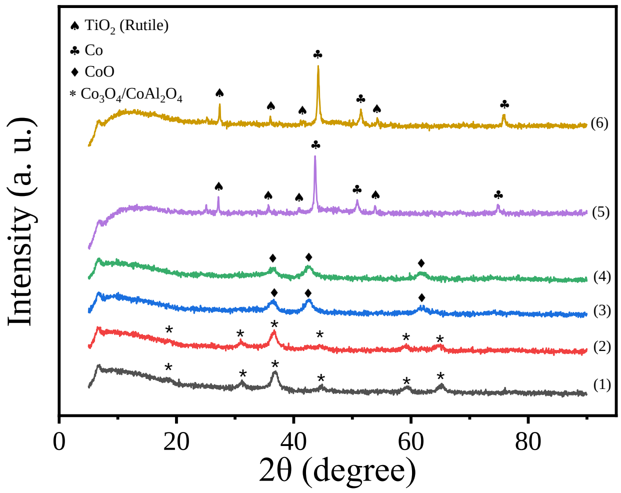

Figure S9. XRD profiles of CoTiAl-MO obtained under H_2 atmosphere at 25 °C (1), 200 °C (2), 300 °C (3), 400 °C (4), 800 °C (5) and after cooling down to room temperature (6).

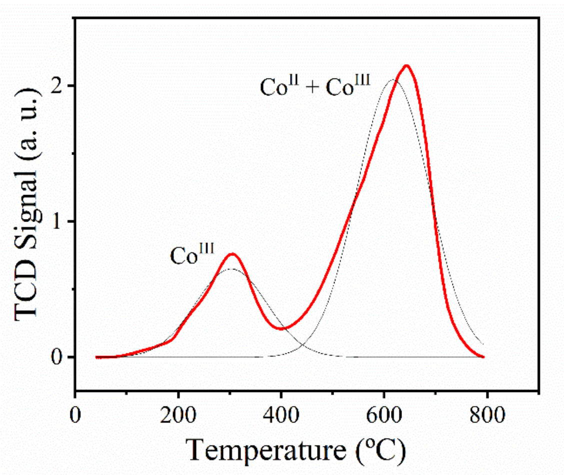

Figure S10. H_2-TPR profile of CoTiAl-MO.

Table S5. Cationic % of Co^{II} and Co^{III} in sample estimated from H_2-TPR data.

	TPR area	Cationic % in sample
Co^{II}	65.5	23.0
Co^{III}	113.8	40.0
Co^{II}+Co^{III}	179.3	63.0

References

1. Y. Qi, L. Song, S. Ouyang, X. Liang, S. Ning, Q. Zhang, J. Ye, Photoinduced Defect Engineering: Enhanced Photothermal Catalytic Performance of 2D Black In_2O_{3-x} Nanosheets with Bifunctional Oxygen Vacancies, Adv Mater 32 (2020) 1903915. https://doi.org/10.1002/adma.201903915.

2. L. Wang, Y. Dong, T. Yan, Z. Hu, F.M. Ali, D.M. Meira, P.N. Duchesne, J.Y.Y. Loh, C. Qiu, E.E. Storey, Y. Xu, W. Sun, M. Ghoussoub, N.P. Kherani, A.S. Helmy, G.A. Ozin, Black indium oxide a photothermal CO2 hydrogenation catalyst, Nat Commun 11 (2020) 1-8. https://doi.org/10.1038/s41467-020-16336-z.

3. N.T. Nguyen, M. Xia, P.N. Duchesne, L. Wang, C. Mao, F.M. Ali, T. Yan, P. Li, Z. Lu, G.A. Ozin, Enhanced CO2 Photocatalysis by Indium Oxide Hydroxide Supported on TiN@TiO2 Nanotubes, Nano Lett. 21 (2021) 1311-1319. https://doi.org/10.1021/acs.nanolett.0c04008.

4. J. Zhao, Q. Yang, R. Shi, G.I.N. Waterhouse, X. Zhang, L. Wu, C. Tung, T. Zhang, FeO–CeO2 nanocomposites: an efficient and highly selective catalyst system for photothermal CO2 reduction to CO, NPG Asia Mater 12 (2020) 1-9. https://doi.org/10.1038/s41427-019-0171-5.

5. J. Ren, S. Ouyang, H. Xu, X. Meng, T. Wang, D. Wang, J. Ye, Targeting Activation of CO2 and H2 over Ru-Loaded Ultrathin Layered Double Hydroxides to Achieve Efficient Photothermal CO2 Methanation in Flow-Type System, Adv. Energy Mater. 7 (2017) 1601657. https://doi.org/10.1002/aenm.201601657.

6. C. Wang, S. Fang, S. Xie, Y. Zheng, Y.H. Hu, Thermo-photo catalytic CO2 hydrogenation over Ru/TiO2, J. Mater. Chem. A 8 (2020) 7390-7394. https://doi.org/10.1039/C9TA13275A.

7. G. Fu, M. Jiang, J. Liu, K. Zhang, Y. Hu, Y. Xiong, A. Tao, Z. Tie, Z. Jin, Rh/Al Nanoantenna Photothermal Catalyst for Wide-Spectrum Solar-Driven CO2 Methanation with Nearly 100% Selectivity, Nano Lett. 21 (2021) 8824-8830. https://doi.org/10.1021/acs.nanolett.1c03215.

8. Y. Tang, S. Wu, Y. Wang, L. Song, Z. Yang, C. Guo, J. Liu, F. Wang, Photo-Assisted Catalytic CO2 Hydrogenation to CO with Nearly 100% Selectivity over Rh/TiO2 Catalysts, Energy Fuels 37 (2023) 539-546. https://doi.org/10.1021/acs.energyfuels.2c03604.

9. Y. Peng, H. Szalad, P. Nikacevic, G. Gorni, S. Goberna, L. Simonelli, J. Albero, N. López, H. García, Co-doped hydroxyapatite as photothermal catalyst for selective CO2 hydrogenation, Applied catalysis. B, Environmental 333 (2023) 122790. https://doi.org/10.1016/j.apcatb.2023.122790.